GEOPHYSICS, VOL. 68, NO. 3 (MAY-JUNE 2003); P. 960–970, 10 FIGS.
10.1190/1.1581068

Removal of wavelet dispersion from ground-penetrating radar data

James D. Irving* and Rosemary J. Knight*

ABSTRACT

Wavelet dispersion caused by frequency-dependent attenuation is a common occurrence in ground-penetrating radar (GPR) data, and is displayed in the radar image as a characteristic "blurriness" that increases with depth. Correcting for wavelet dispersion is an important step that should be performed before GPR data are used for either qualitative interpretation or the quantitative determination of subsurface electrical properties. Over the bandwidth of a GPR wavelet, the attenuation of electromagnetic waves in many geological materials is approximately linear with frequency. As a result, the change in shape of a radar pulse as it propagates through these materials can be well described using one parameter, Q^*, related to the slope of the linear region. Assuming that all subsurface materials can be characterized by some Q^* value, the problem of estimating and correcting for wavelet dispersion becomes one of determining Q^* in the subsurface and deconvolving its effects using an inverse-Q filter. We present a method for the estimation of subsurface Q^* from reflection GPR data based on a technique developed for seismic attenuation tomography. Essentially, Q^* is computed from the downshift in the dominant frequency of the GPR signal with time. Once Q^* has been obtained, we propose a damped-least-squares inverse-Q filtering scheme based on a causal, linear model for constant-Q wave propagation as a means of removing wavelet dispersion. Tests on synthetic and field data indicate that these steps can be very effective at enhancing the resolution of the GPR image.

INTRODUCTION

The attenuation of electromagnetic (EM) waves in many geological materials is strongly dependent upon frequency in the ground-penetrating radar (GPR) frequency range; higher frequencies are attenuated much more quickly than lower ones during propagation. As a result, the GPR wavelet often undergoes a significant change in shape as it travels through the subsurface, and reflections received at later times are noticeably broader than those received at earlier times. This phenomenon is known as wavelet dispersion. In the GPR image, it is displayed as a characteristic "blurriness" or lack of resolution that increases with time/depth.

Correcting for wavelet dispersion in GPR data is important for a number of reasons. Qualitatively, it is desirable to have a high-resolution, well-focused GPR image for interpretation purposes. Quantitatively, the removal of wavelet dispersion is a necessary step before applying signal processing methods, such as migration and spiking deconvolution, that are based upon the assumption of a stationary wavelet. Indeed, past attempts at applying these processing methods, which are standard in the seismic industry, to dispersive GPR data have proven largely unsuccessful (e.g., LaFlèche et al., 1991; Rees and Glover, 1992; Powers, 1995). Further, since these methods ultimately lead to the recovery of the earth's reflectivity, it is clear that correcting for wavelet dispersion is important before GPR data are used for the estimation of subsurface electrical properties.

While numerous studies have addressed the issue of dispersion in GPR data and the importance of accounting for it when forward modeling (e.g., Arcone, 1981; Powers and Olhoeft, 1994; Annan, 1996; Carcione, 1996; Xu and McMechan, 1997; Hollender and Tillard, 1998), relatively little research has been published on the problem of removing wavelet dispersion from GPR data. Turner (1994) was the first to consider this problem, presenting an algorithm to correct for wavelet dispersion in GPR data based on prior knowledge of the earth's attenuation behavior with frequency. In a subsequent paper, Turner and Siggins (1994) showed that, over the bandwidth of a GPR pulse, the attenuation of a number of earth materials could be adequately characterized using a parameter known as Q^*, which is closely related to the seismic quality factor, Q. Baño (1996a,b) also justified theoretically the use of a constant-Q assumption in GPR under certain conditions, and presented inverse-Q filtering as a means of removing wavelet dispersion.

Manuscript received by the Editor March 25, 2002; revised manuscript received September 26, 2002.
*Formerly University of British Columbia, Department of Earth and Ocean Sciences, Vancouver, British Columbia V6T 1Z4, Canada; presently Stanford University, Department of Geophysics, Mitchell Building, Stanford, California 94305-2215. E-mail: jdirving@pangea.stanford.edu; rknight@pangea.stanford.edu

What remains absent from all of these publications, however, is an effective method for estimating the frequency-dependent attenuation behavior of the earth from GPR data. Clearly, this must be known before we can correct for wavelet dispersion. A convincing field example illustrating the importance of removing wavelet dispersion from GPR data is also absent from the literature.

In this paper, we investigate further the results of Turner and Siggins (1994) and conclude that the frequency-dependent attenuation behavior of many geological materials can be adequately described using their parameter, Q^*, over the bandwidth of a GPR wavelet. Assuming that all materials encountered in the subsurface can be characterized in this manner, the problem of estimating and correcting for wavelet dispersion in GPR data becomes one of determining subsurface Q^* and deconvolving its effects using an inverse-Q filter. Building on the frequency shift method of Quan and Harris (1997), we develop a practical method for Q^* estimation from reflection GPR data that involves examination of the change in frequency content of a data set with time. We next introduce a damped-least-squares inverse-Q filtering scheme based on a causal, linear model for constant-Q wave propagation as an effective means of correcting for wavelet dispersion. As an example, we show the successful application of these techniques to a 100-MHz field data set collected near Langley, British Columbia, Canada.

ELECTRICAL PROPERTIES OF GEOLOGICAL MATERIALS

Relevant equations

Away from the immediate vicinity of the transmitter antenna, radar waves in the subsurface can be approximated by plane waves. For monochromatic EM plane waves traveling in the z-direction, we have

$$\tilde{\mathbf{E}}(z,t) = \tilde{\mathbf{E}}_0 e^{i(\omega t - kz)}, \tag{1}$$

where $\tilde{\mathbf{E}}$ is the complex electric field vector, $\tilde{\mathbf{E}}_0$ is the complex amplitude containing the wave polarization and phase, ω is the angular frequency, and

$$k = \frac{\omega}{v} - i\alpha \tag{2}$$

is the wavenumber.

We adopt the convention of Fuller and Ward (1970) and define the two properties governing EM wave propagation in earth materials as the complex dielectric permittivity, given by

$$\epsilon^*(\omega) = \epsilon'(\omega) - i\epsilon''(\omega), \tag{3}$$

and the complex electrical conductivity, given by

$$\sigma^*(\omega) = \sigma'(\omega) + i\sigma''(\omega). \tag{4}$$

At GPR frequencies, the electrical conductivity is assumed to be a fixed, frequency-independent, real value equal to the dc conductivity (Keller, 1987; Olhoeft and Capron, 1994; Xu and McMechan, 1997). Thus, we have

$$\sigma'(\omega) = \sigma_{dc}, \tag{5}$$

$$\sigma''(\omega) = 0. \tag{6}$$

Note that the above formulation neglects any dependence of EM wave propagation on the magnetic permeability μ. Most geological materials encountered with GPR do not contain significant amounts of magnetic materials. We have thus chosen to treat μ as constant and equal to its value in free space, μ_0 (Topp et al., 1980; Xu and McMechan, 1997; Hollender and Tillard, 1998).

The phase velocity, v, and attenuation, α, in equation (2) are now given by the following expressions:

$$v = \left[\frac{\mu_0 \epsilon_{ef}}{2} \sqrt{1 + \left(\frac{\sigma_{ef}}{\omega \epsilon_{ef}} \right)^2} + 1 \right]^{1/2}, \tag{7}$$

$$\alpha = \omega \left[\frac{\mu_0 \epsilon_{ef}}{2} \sqrt{1 + \left(\frac{\sigma_{ef}}{\omega \epsilon_{ef}} \right)^2} - 1 \right]^{1/2}, \tag{8}$$

where ϵ_{ef} and σ_{ef} are the real-valued, effective, dielectric permittivity and electrical conductivity, respectively, given as follows:

$$\epsilon_{ef} = \epsilon'(\omega), \tag{9}$$

$$\sigma_{ef} = \sigma_{dc} + \omega \epsilon''(\omega). \tag{10}$$

An important parameter in EM applications is the loss tangent, given by

$$\tan \delta = \frac{\sigma_{ef}}{\omega \epsilon_{ef}}. \tag{11}$$

For GPR to serve as an effective tool for high-resolution subsurface imaging, the loss tangent must be less than 1. This corresponds to the case where energy storage mechanisms (i.e., polarization) dominate over energy loss mechanisms (i.e., conduction).

EXPERIMENTAL RESULTS

Using laboratory measurements, Turner and Siggins (1994) showed that, over the bandwidth of a GPR wavelet, the attenuation of EM waves in a number of dry sands and rocks could be adequately characterized as a linear function of frequency. Since velocity dispersion is often small over the GPR range and can be calculated from the attenuation behavior by invoking causality (e.g., Futterman, 1962; Aki and Richards, 1980), they concluded that the change in shape of a radar pulse in these materials could be well described using a single parameter. This parameter is related to the slope of the attenuation versus frequency curve in the region of interest. In order to assess the generality of these results, we have used published dielectric permittivity data to calculate the attenuation and velocity for a number of other geological materials over the radar frequency range of 10 to 1000 MHz.

Figure 1 shows the calculated attenuation and velocity for a variety of soils and rocks whose permittivity measurements were fitted using the Cole-Cole formula (Cole and Cole, 1941). We used the published dielectric fitting parameters to obtain permittivity versus frequency, which was then used in equations (7)–(10) to obtain the velocity and attenuation as a function of frequency. The Cole-Cole formula is derived through the addition of a distribution parameter over the time constant in the Debye (1945) relaxation equation. It has been used with much success in the GPR frequency range to fit

permittivity measurements (Taherian et al., 1990; Olhoeft and Capron, 1993), and is given by

$$\epsilon^*(\omega) = \epsilon_\infty + \frac{\epsilon_s - \epsilon_\infty}{1 + (i\omega\tau)^a}, \tag{12}$$

where ϵ_∞ and ϵ_s are the high- and low-frequency limiting values of $\epsilon'(\omega)$, τ is the time constant, and a is the distribution parameter that ranges between 0 and 1.

Figure 2 shows the calculated attenuation and velocity versus frequency for a variety of rocks whose permittivity measurements were fitted using the Jonscher parameterization (Hollender and Tillard, 1998). Based on the work of Jonscher (1977), this parameterization assumes a power law dependence upon frequency of the real and imaginary parts of the permittivity, and can be expressed as

$$\epsilon^*(\omega) = \epsilon_r \left(\frac{\omega}{\omega_r}\right)^{n-1} \left[1 - \cot\left(\frac{n\pi}{2}\right)\right] + \epsilon_\infty, \tag{13}$$

where $\epsilon_r = \epsilon'(\omega) - \epsilon_\infty$ at the reference frequency ω_r, and $n - 1$ is the power law exponent.

Note in Figures 1 and 2 that, in general, the attenuation displays a high level of frequency dependence over the GPR range. This indicates that there will be significant broadening in the GPR wavelet during propagation through these materials. The slow increase in velocity over most of the GPR band shows that the change in shape of a radar pulse due to velocity dispersion alone will be minimal in these substances.

Of importance in our study are the characteristics of the attenuation and velocity curves in Figures 1 and 2 over the bandwidth of a GPR wavelet. Current GPR systems radiate wavelets with bandwidths of approximately two octaves (Hollender and Tillard, 1998). Over any two octave range, Figures 1 and 2 demonstrate that the attenuation can be reasonably approximated as a linear function of frequency, and the velocity can be well characterized as constant. Thus, in accordance with Turner and Siggins (1994), a reasonable approach is to quantify wavelet dispersion in these materials using a single parameter.

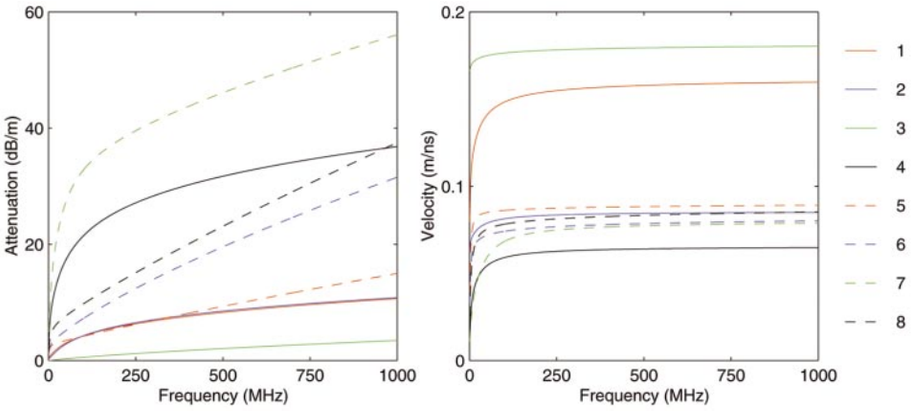

FIG. 1. Attenuation and velocity calculated as a function of frequency for a variety of geological materials whose dielectric permittivities were fitted using the Cole-Cole formula: (1) sandy soil (natural state), (2) sandy soil (saturated) (Olhoeft and Capron, 1993); (3) clay soil (dry), (4) clay soil (30.18 wt% water) (Olhoeft and Capron, 1994); (5) and (6) limestone saturated with brine, (7) and (8) sandstone saturated with brine (Taherian et al., 1990).

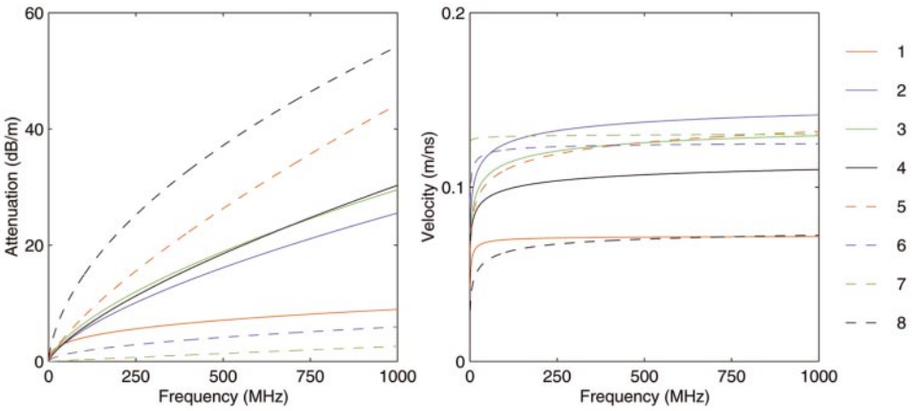

FIG. 2. Attenuation and velocity calculated as a function of frequency for a variety of rocks whose dielectric permittivities were fitted using the Jonscher parameterization: (1) limestone (freshwater saturated), (2) andesite, (3) shale, (4) gabbro, (5) siltstone, (6) granite (freshwater saturated), (7) granite (dry), (8) schist (measured perpendicular to the schistocity) (Hollender and Tillard, 1998).

Q and Q^* parameters

To describe the change in shape of a GPR wavelet in materials whose attenuation and velocity behaviors are similar to those in Figures 1 and 2, Turner and Siggins (1994) introduced the parameter Q^*, defined as

$$Q^* = \frac{1}{2v}\left(\frac{\Delta\alpha}{\Delta\omega}\right)^{-1}, \tag{14}$$

where, in the region of interest (i.e., the bandwidth of the GPR wavelet), v is the approximately constant value for the velocity, and $\Delta\alpha/\Delta\omega$ is the slope of the attenuation versus frequency curve. Q^* is a generalization of the quality factor, Q, commonly seen in seismic studies (e.g., Aki and Richards, 1980):

$$Q = \frac{\omega}{2v\alpha}. \tag{15}$$

When the line approximating the attenuation extrapolates to zero at zero frequency, the two parameters are equivalent. Also, Q^* and Q describe the same change in wavelet shape that occurs during propagation, except for a difference in total amplitude (Turner and Siggins, 1994); thus values for Q^* can be compared directly with those for Q in regards to wavelet dispersion. Based on their laboratory measurements, Turner and Siggins concluded that Q^* for GPR should lie somewhere between 2 and 30. This is roughly an order of magnitude lower than the range of values typically given for seismic Q, which indicates that wavelet dispersion is far more pronounced in GPR data than in seismic data.

Based on the work of Turner and Siggins (1994) and the results shown in Figures 1 and 2, we believe that Q^* values calculated over the bandwidth of a GPR wavelet can adequately describe wavelet dispersion in many, if not most, geological materials encountered with GPR. Consequently, we make the fundamental assumption in this work that all subsurface materials can be characterized in this manner. When this is the case, the problem of estimating and correcting for wavelet dispersion in GPR data becomes one of determining Q^* in the subsurface and deconvolving its effects using an inverse-Q filter.

It should be noted that, although constant-Q is often used to describe seismic wave propagation and attenuation (e.g., Strick, 1967; Stacey et al., 1975; Kjartansson, 1979), we must use Q^* in the GPR case because the line approximating the attenuation of EM waves in earth materials does not, in general, pass through the origin (see Figures 1 and 2). For EM waves, Q is closely related to the loss tangent as follows (von Hippel, 1962):

$$Q = \frac{1}{\tan\delta}. \tag{16}$$

This quantity has been shown in a number of studies to be rarely constant in the GPR range (Xu and McMechan, 1997; Hollender and Tillard, 1998). Although Bano (1996a) justified the use of a constant-Q assumption for GPR, we believe that this result lacks sufficient generality because he neglected both the dc conductivity and the high-frequency limiting value of the real part of the permittivity, ϵ_∞, in his derivations.

ESTIMATION OF Q^* FROM GPR DATA

The frequency shift method

A number of methods have been mentioned in the literature for the estimation of subsurface Q or Q^* from GPR data. Turner (1994), for example, stated that it may be possible to obtain Q^* from pulse-width or rise-time measurements, as has been done in seismic laboratory and tomography experiments (Gladwin and Stacey, 1974; Kjartansson, 1979). Baño (1996a), on the other hand, proposed that Q could be determined in GPR by comparing wavelets recorded at the receiver with groups of synthetically attenuated ones. Another common method for Q estimation in seismic studies is the spectral ratio technique (Toksöz et al., 1979). Although all of these methods are completely valid in theory, we have found they are impractical for use on most reflection GPR data sets because they require the accurate isolation of individual reflections on a trace. Unless reflection events are spaced widely apart in time, and noise levels in the data are very low, this is an extremely difficult, if not impossible, task. To avoid this problem, we propose a technique for the estimation of subsurface Q^* from GPR data that builds on the frequency shift method of Quan and Harris (1997).

Developed for seismic attenuation tomography, the frequency shift method uses the principle that, as a wavelet propagates and broadens due to frequency-dependent attenuation, the centroid of its amplitude spectrum undergoes a gradual downshift in frequency. This downshift is related to Q (and thus Q^*) as follows:

$$f_S - f_R = C\int_{ray}\frac{\pi}{vQ}d\ell, \tag{17}$$

where the integral is taken along the raypath, and f_S and f_R are the centroid frequencies of the source and received wavelet amplitude spectra, $S(f)$ and $R(f)$, given by

$$f_S = \frac{\int_0^\infty f S(f)df}{\int_0^\infty S(f)df}, \tag{18}$$

$$f_R = \frac{\int_0^\infty f R(f)df}{\int_0^\infty R(f)df}. \tag{19}$$

For a source spectrum that is approximately Gaussian in shape, Quan and Harris (1997) showed that the parameter C in equation (17) is equal to the spectrum variance, defined as

$$\sigma_S^2 = \frac{\int_0^\infty (f - f_S)^2 S(f)df}{\int_0^\infty S(f)df}, \tag{20}$$

which remains constant during propagation. They also derived expressions for C for boxcar and triangular-shaped source spectra.

To formulate these results for the estimation of Q^* from reflection GPR data, we first assume that the only cause of amplitude spectral variation in a propagating GPR

pulse is frequency-dependent attenuation. To a large extent, geometrical energy spreading is independent of frequency (Turner and Siggins, 1994). In addition, although it has been shown that reflection and transmission at subsurface interfaces can result in significant changes in the shape of a radar wavelet (Hollender and Tillard, 1998), we believe that this is the exception, rather than the norm, in environments well-suited to GPR. It is also unlikely that interface reflection and transmission effects will cause the progressive broadening of arrivals down a trace that is characteristic of frequency-dependent attenuation.

It should be noted that we cannot neglect the effects of scattering in GPR data; both multipathing and volume scattering within a medium can result in significant pulse broadening with time down a trace (O'Doherty and Anstey, 1971; Olhoeft, 1998). Consequently, any estimates of Q^* that we obtain will contain a contribution from the component of scattering attenuation that is linear with frequency. This is not a problem for our purposes, however, because inverse-Q filtering will simply correct for the combined effects of intrinsic and scattering attenuation.

Consider now the case of two horizontal interfaces in the subsurface separated by a layer of constant Q^* material. Using equation (17), the difference between the centroid frequencies of the two wavelets reflected from these interfaces can be expressed as

$$f_{R_2} - f_{R_1} = -\frac{C\pi}{Q^*}(t_2 - t_1), \tag{21}$$

where t_1 and t_2 refer to the arrival times of the wavelets on a trace. If we now make the assumptions that (1) traces recorded using GPR contain a high density of reflections in time (this is often the case), and (2) the subsurface can be adequately described by one or a small number of general values for Q^* with depth, then the above result yields

$$Q^* = -C\pi\left(\frac{\Delta f}{\Delta t}\right)^{-1}. \tag{22}$$

That is, general values for subsurface Q^* can be obtained from reflection GPR data from the slope of a best-fit line to a centroid frequency versus time curve. This curve is determined by calculating the centroid frequency of the local amplitude spectrum at each time down a trace. In the situation where only one general value for Q^* is present with depth, the curve will exhibit only one slope. If two regions having considerably different Q^* values are present in the subsurface, then the curve should exhibit two distinct slopes, and so on. Notice that, by estimating Q^* in this manner, we largely avoid the problems associated with isolating individual reflections on a trace because Q^* is not obtained from particular reflection events. Instead, our method estimates Q^* from the general trend in spectral character of a GPR trace, averaging over all possible amplitude spectra.

Time-frequency analysis

To obtain the amplitude spectrum at each time down a trace (i.e., a trace's time-frequency representation), we use the S-transform (Stockwell et al., 1996; Theophanis and Queen, 2000). The S-transform examines the time-frequency character of a signal by integrating that signal at each point in time with a series of windowed harmonics of various frequencies. This is expressed as follows:

$$ST(f,\tau) = \int_{-\infty}^{\infty} h(t)\frac{|f|}{\sqrt{2\pi}}e^{-\frac{(\tau-t)^2 f^2}{2}}e^{-i2\pi f t}dt, \tag{23}$$

where $h(t)$ is the signal being analyzed, τ is a translation parameter, and the two exponentials represent the window and harmonic functions, respectively. To compute the transform, the window function is shifted in time by τ down the signal and a range of frequencies is repeatedly analyzed. The window function, a Gaussian with variance $1/f^2$, scales in width according to the frequency being examined.

We have found that, for Q^* estimation using our variation of the frequency shift method, the S-transform is superior to other time-frequency analysis tools such as the short-time Fourier transform (STFT) and the wavelet transform (WT). Because it employs a constant window width for all frequencies, the STFT is not well-suited to the analysis of signals that contain different-scale features, such as a dispersive GPR trace. In other words, one may question what window width is appropriate for the analysis of a trace whose reflections gradually change in scale as time increases. Also, short time-scale features such as spurious noise and interference effects tend to become included in many spectra down a trace with the STFT, and therefore have the potential to significantly influence estimates of Q^*. With the WT, we avoid these shortcomings because the analysis of a signal is performed using scaled and translated versions of a "mother wavelet" function; however, this also has limitations as it involves the rather difficult decision of choosing the mother wavelet, and also the problem of having to convert measures of scale into frequency.

The S-transform can be regarded as a hybrid of the WT and the Gabor transform, a version of the STFT in which a Gaussian window function is employed (Gabor, 1946). Like the STFT, the S-transform analyzes a signal using windowed harmonics, and thus yields a true measure of frequency. Like the WT, features are analyzed with a resolution suited to their scale because the effective width of the Gaussian window changes with frequency. High frequencies are analyzed using a short time window with the S-transform; low frequencies are analyzed using longer time windows. Many researchers also believe that the Gaussian window produces the optimum spectral shape for a given bandwidth (e.g., Deregowski, 1971).

Synthetic example

Figure 3 shows the construction of a very simple, synthetic GPR trace that we used to test our Q^* estimation procedure. First, a reflectivity series was created by randomly distributing 40 reflection coefficients in time between 20 and 350 ns (Figure 3a). Using the constant-Q transfer function given by equation (27), this reflectivity series was then attenuated assuming a single subsurface value of $Q^* = 30$. The attenuated series, which represents the impulse response of a lossy earth, is shown in Figure 3b. Note how the attenuated reflection spikes broaden significantly as time increases; near the end of the signal, many of them become indistinguishable from one another. To obtain the synthetic trace in Figure 3c, the attenuated series was convolved with a zero-phase wavelet having a Gaussian amplitude spectrum with -20 dB set at 80 and 320 MHz. This "Gaussian wavelet" has a peak frequency of 200 MHz,

and a bandwidth of approximately two octaves. Based on our observations, we believe that it reasonably approximates a typical 200-MHz GPR pulse. It should be noted that, by choosing $Q^* = 30$, we have designed a relatively rigorous test for our estimation procedure, as this is the upper limit of the range for Q^* suggested by Turner and Siggins (1994). Accurate determination of Q^* will be most difficult for higher Q^* values, when the slope of the centroid frequency versus time curve is small.

Figure 4 shows the time-frequency representation of the synthetic trace in Figure 3c, obtained using the S-transform. In the time-frequency plane, a clear downshift in the dominant frequency of the trace with time is evident as a result of wavelet dispersion; the dominant frequency drops from 200 MHz to approximately 100 MHz over the interval shown. This figure also demonstrates the resolution properties of the S-transform. High frequencies are resolved well in time but poorly in frequency because a narrow analyzing window is used. Low frequencies, on the other hand, can be seen to be resolved well in frequency but poorly in time due to the use of a wide analyzing window. We have found that these resolution properties do not significantly affect the estimates of Q^* obtained using our method.

The S-transform results from Figure 4 were fed into a discretized version of equation (18) in order to calculate the centroid frequency of the synthetic trace in Figure 3c at each point in time. Figure 5a shows the resulting centroid frequency versus time curve. Because the trace contains a high density of reflections and there is only one value for Q^* in the subsurface, the downshift exhibited by this curve is approximately linear. To estimate Q^*, a least-squares regression line was fit to the curve. The slope of this line (shown on the plot) is -0.31 MHz/ns. This value, along with the known value of $C = \sigma^2 = 3125$ for our input Gaussian wavelet, were used in equation (22) to obtain $Q^* = 31.7$. Since this result is very close to the true value of $Q^* = 30$, it can be concluded that our Q^* estimation procedure was very successful for this example.

To gain further insight into our Q^* estimation algorithm, we also computed the centroid frequency versus time curves for the synthetic trace in Figure 3c after inverse-Q filtering to remove wavelet dispersion. Figure 5b shows the curve obtained after filtering using the correct value of $Q^* = 30$. Because we have properly removed wavelet dispersion from the trace, this curve is approximately flat. For comparison, Figures 5c and 5d show the centroid frequency versus time curves after inverse-Q filtering using $Q^* = 20$ and $Q^* = 40$, respectively. Here, we see that inverse-Q filtering with too low a value for Q^* will overcompensate for frequency-dependent attenuation, resulting in a centroid frequency versus time curve that has positive slope (i.e., high frequencies are preferentially boosted too much in the filtered output). Conversely, inverse-Q filtering using a value for Q^* that is too high results in a centroid frequency curve with negative slope, indicating that we have only partially corrected for wavelet dispersion. These results suggest that we can verify our success in removing wavelet dispersion from a trace by looking at the centroid frequency versus time curve of the trace after inverse-Q filtering.

It is important to note that there are a number of sources of potential error in our Q^* estimation procedure. First, it can be seen from Figure 5 that centroid frequency versus time curves, in general, show a high degree of variability about the main trend, and also tend to dive towards zero in regions of the signal where there are no reflections (best shown around 190 and 250 ns). This can clearly influence the slope of a best-fit line, thus affecting estimates of Q^*. However, we can significantly

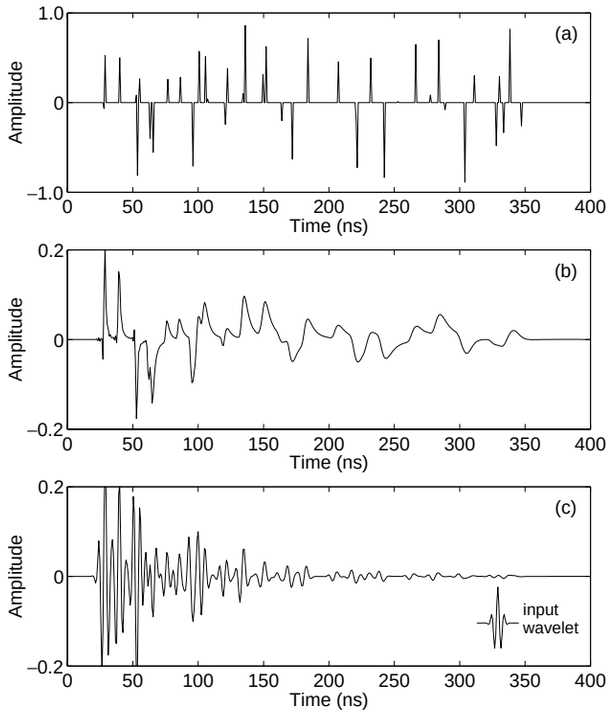

FIG. 3. Creation of the synthetic GPR trace used to test our Q^* estimation procedure. (a) random reflectivity series, (b) reflectivity series in (a) attenuated using constant $Q^* = 30$, (c) the synthetic GPR trace, obtained by convolving the attenuated reflectivity series in (b) with a 200-MHz Gaussian wavelet (see text).

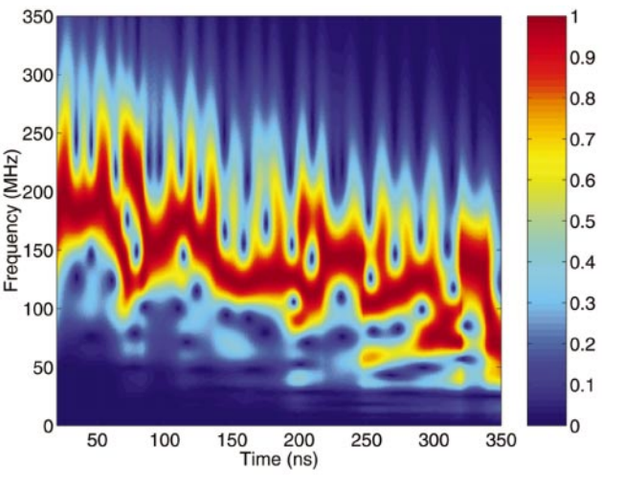

FIG. 4. S-transform time-frequency representation of the synthetic trace from Figure 3. Only the region of the trace containing signal (from 20 to 350 ns) was analyzed. Individual spectra at each time have been normalized to their maximum values in order to better show the downward trend in the dominant frequency of the signal with time.

reduce errors related to these phenomena if we compute one best-fit line through a number of centroid frequency versus time curves obtained from different traces, but representative of the same subsurface material. Secondly, in practice, we will not know beforehand the value of C in equation (22), which in the case of our synthetic example was simply the variance of the source wavelet. Thus C must be estimated from our data, which could be a significant source of error in Q^*. However, even if our estimate of Q^* is inaccurate, we can easily check whether we have properly removed wavelet dispersion by determining whether the centroid frequency versus time curve after inverse-Q filtering is indeed flat.

INVERSE-Q FILTERING

Constant-Q wave propagation

As mentioned previously, Q^* and Q describe the same change in wavelet shape that occurs during propagation, except for a difference in total amplitude. As a result, once Q^* in the subsurface has been determined, we can correct for wavelet dispersion in GPR data by inverse-Q filtering, a technique commonly applied to seismic data in order to remove the effects of propagation through constant-Q materials. To satisfy causality, frequency-dependent attenuation must be accompanied by velocity dispersion (Aki and Richards, 1980). Therefore, any realistic inverse-Q filter must correct for slight changes in wavelet shape caused by variations in velocity with frequency, in addition to wavelet broadening resulting from frequency-dependent attenuation. To inverse-Q filter GPR data, we consider a causal, linear model for constant-Q wave propagation based on a power law formula for the wavenumber k (e.g., Kjartansson, 1979; Bickel and Natarajan, 1985), which yields attenuation nearly linear with frequency and velocity nearly constant over a wide bandwidth:

$$v = v_0\left(\frac{\omega}{\omega_0}\right)^{\gamma}, \tag{24}$$

$$\alpha = \frac{\omega}{2v_0 Q}\left(\frac{\omega}{\omega_0}\right)^{-\gamma}, \tag{25}$$

where v_0 is the phase velocity at the arbitrary reference frequency ω_0, and γ is given by

$$\gamma = \frac{2}{\pi}\tan^{-1}\left(\frac{1}{2Q}\right). \tag{26}$$

Substituting the above results into the wave propagation operator e^{-ikz} allows us to formulate the following frequency domain expression for the forward-Q propagation filter, which accounts for all effects of velocity and attenuation in a constant-Q medium:

$$U(\omega, t_j) = \exp\left[-t_j\,\omega\left(\frac{\omega}{\omega_0}\right)^{-\gamma}\left(\frac{1}{2Q} + i\right)\right]. \tag{27}$$

Equation (27) is the transfer function that turns an impulse at time $t = 0$ into an attenuated impulse arriving around time t_j on a trace. For the case of no attenuation (i.e., infinite Q and hence $\gamma = 0$), the expression becomes simply a linear phase shift which translates the impulse at $t = 0$ to time t_j.

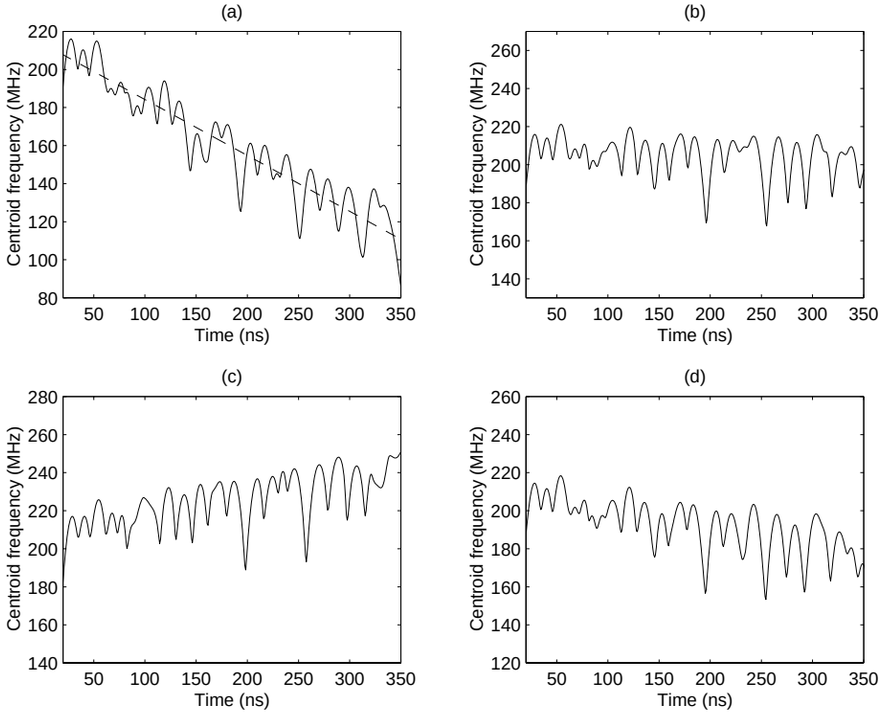

FIG. 5. Centroid frequency versus time curves for the synthetic trace in Figure 3, before and after inverse-Q filtering to remove wavelet dispersion: (a) before inverse-Q filtering (slope of best-fit line is −0.31 MHz/ns), (b) after inverse-Q filtering using the correct value of $Q = 30$, (c) after inverse-Q filtering using $Q = 20$, (d) after inverse-Q filtering using $Q = 40$.

Filter design

Note that the inverse of equation (27) is an increasing exponential in time and frequency. To design a stable inverse-Q filter in the presence of noise, we therefore use the damped-least-squares inverse of this equation, given by (e.g., Berkhout, 1982)

$$H(\omega, t_j) = \frac{U^*(\omega, t_j)}{|U(\omega, t_j)|^2 + \Delta(\omega)}, \tag{28}$$

where $*$ and $|\cdot|$ denote the complex conjugate and modulus, respectively, and $\Delta(\omega)$ is a damping or regularization parameter whose value controls the trade-off between having an accurate inverse and avoiding the amplification of noise in the filtered output. From a Bayesian perspective, assuming a Gaussian model for the noise in our GPR data and also a Gaussian prior for the attenuation-free trace, the regularization parameter can be viewed as the ratio of the noise variance to the variance of the attenuation-free trace. This may also be interpreted as the inverse square of the signal-to-noise ratio in our data at time $t = 0$, before any attenuation has occurred. For this reason, we define

$$\Delta(\omega) = \frac{1}{SN_0(\omega)^2}, \tag{29}$$

where $SN_0(\omega)^2$ is an estimate of the initial signal-to-noise ratio at $t = 0$ as a function of frequency. Note that, by defining the regularization parameter in this manner, we can easily avoid boosting regions of the input trace's frequency spectrum that are outside the bandwidth of the GPR source wavelet; $\Delta(\omega)$ is simply made large for these frequencies.

Just as $U(\omega, t_j)$ converts an impulse at $t = 0$ into an attenuated impulse arriving around $t = t_j$, $H(\omega, t_j)$ turns an attenuated impulse around time t_j into its corresponding reflection spike at $t = 0$. Thus, to perform inverse-Q filtering, $H(\omega, t_j)$ is computed for each time t_j down the input trace. Each $H(\omega, t_j)$ is then applied separately to the trace, and the samples at $t = 0$ are extracted. These samples are then put together to form the inverse-Q filtered output. It should be noted that variations in Q^* with depth can be easily incorporated into our inverse-Q filter through the effective Q approach, whereby an effective Q value calculated for each depth is used to represent the attenuation effect of the variable Q structure above that depth (Varela et al., 1993).

Synthetic example

We now show the results of applying our inverse-Q filter to a synthetic attenuated reflectivity series with added noise. Figure 6a shows the original reflectivity series, consisting of 12 reflection spikes of random amplitude separated by different amounts in time. As before, this series was attenuated assuming a constant value of $Q^* = 30$. Gaussian random noise with a standard deviation equal to 2% of the maximum value of the original reflectivity series was then added to create the trace shown in Figure 6b. Figure 6c shows the result of inverse-Q filtering the noisy attenuated reflectivity series using $Q = 30$ and $SN_0(\omega) = 50$. The resolution of the trace is greatly improved upon inverse-Q filtering. Reflections are greatly reduced in width, and all of the individual spikes in the original reflectivity series (with the exception of the one near 220 ns) can be easily distinguished. There remains, however, a noticeable amount of broadening in the reflections of Figure 6c, even after the filtering. This is because, in the presence of noise, we can never obtain a perfect inverse-Q filtered result; regions of a trace's time-frequency spectrum where noise is dominant cannot be boosted in a stable manner. However, our inverse-Q filter clearly does a good job of removing most of the wavelet dispersion from the noisy input trace. Furthermore, in working with real data, the shortcomings of inverse-Q filtering noisy data (i.e., having a filtered result that still contains dispersion) will not be as evident because we will be dealing with a finite bandwidth wavelet, not an infinite bandwidth impulse.

APPLICATION TO FIELD DATA

The techniques described above for the estimation and removal of wavelet dispersion in GPR data were applied to a 100-MHz field data set collected near Langley, British Columbia, Canada. The field site consists of an unconfined sand and gravel aquifer underlain by a conductive clay, which was not penetrated with the radar. The data were acquired using a Sensors & Software PulseEkko IV GPR system, with the transmitter and receiver antennas separated a fixed distance of 1 m. A spatial sampling interval of 0.2 m and a time sampling interval of 0.8 ns were used. Preprocessing included residual median filtering to remove the low-frequency "wow" from the radar data upon which the reflection signal is superimposed, time-zero shifting to align traces in the data set on the first

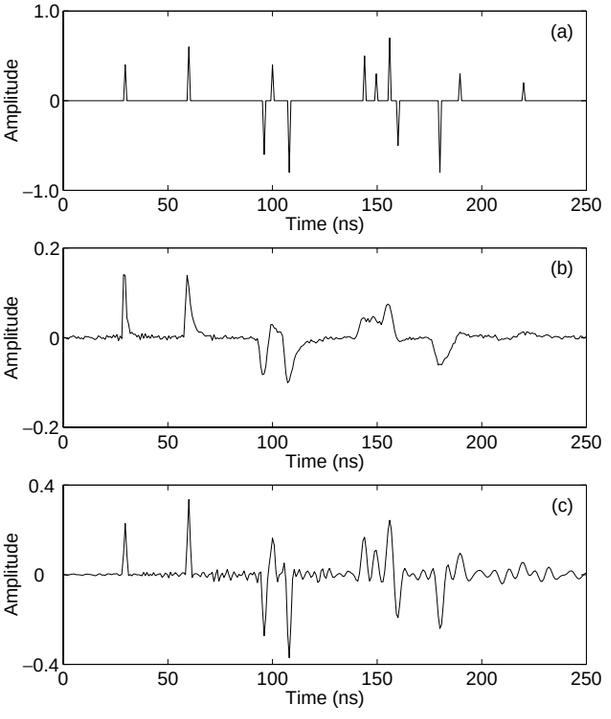

FIG. 6. Synthetic example showing application of our inverse-Q filtering algorithm to a noisy, attenuated reflectivity series: (a) input reflectivity series, (b) reflectivity series in (a) attenuated using constant $Q = 30$ and 2% noise added, (c) noisy attenuated series in (b) after inverse-Q filtering using $Q = 30$, $SN_0(\omega) = 50$.

arrival, and an approximate correction for geometrical energy spreading. Since the ground along the survey line was flat, no correction for topography was necessary. A constant velocity of 0.1 m/ns was used to convert time into an approximate depth.

Figure 7 shows a section of the Langley data from 50 to 120 m where the top of the clay layer, which is marked by rapid attenuation of the GPR signal, can be seen to increase in depth from left to right. For this plot, a standard, frequency-independent, time-varying, exponential gain was applied to the data in an attempt to correct for attenuation. The presence of wavelet dispersion in the data can be seen as a lack of resolution or blurriness in the image that increases with depth. Clearly, a more accurate frequency-dependent correction for attenuation is needed. Given that most traces across the profile exhibit a high density of reflections, and that the reflections all originate from within a common subsurface unit (the sand and gravel aquifer), the data set is a good candidate for Q^* estimation using our variation of the frequency shift method.

To estimate a general value for Q^* in the sand and gravel aquifer, 100 traces between 100 and 120 m (where the thickness of the aquifer is greatest) were analyzed using the S-transform over the approximate bandwidth of the 100-MHz GPR source wavelet. This was estimated to lie between 20 and 180 MHz. A smooth, time-varying exponential gain was applied to the data before computing the transform to somewhat balance amplitudes down the traces. Figure 8 shows the calculated centroid frequency versus time curves for the 100 traces analyzed. Only times between 20 and 350 ns were considered in order to avoid the direct air and ground arrivals at the beginning of the traces, and the regions dominated by noise at late times. All of the curves can be seen to have a similar trend: they exhibit a significant downshift in time due to wavelet dispersion. This downshift was fitted using a single line having slope −0.081 MHz/ns. Clearly, fitting all of the curves with one best-fit line yields a much better estimate of the general slope than fitting centroid frequency versus time curves individually. To determine the

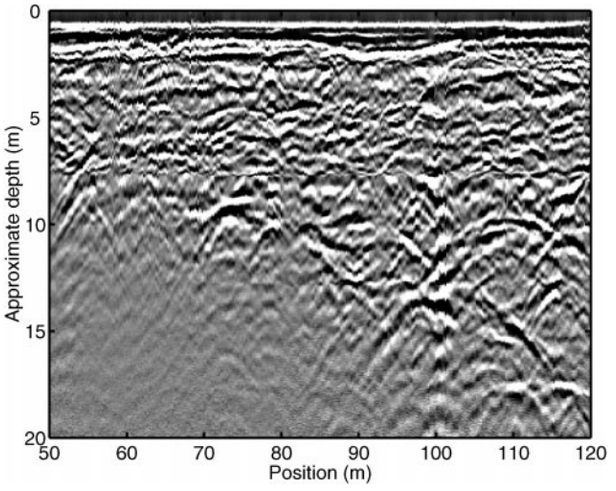

FIG. 7. Langley 100-MHz GPR data before correcting for wavelet dispersion.

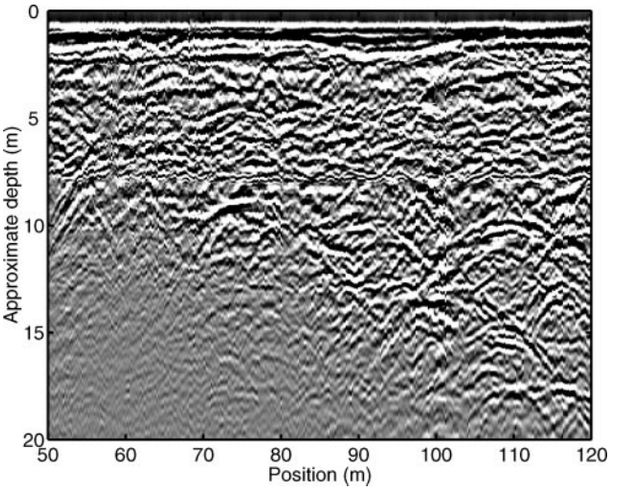

FIG. 9. Langley 100-MHz GPR data after correcting for wavelet dispersion by inverse-Q filtering, Q = 45.

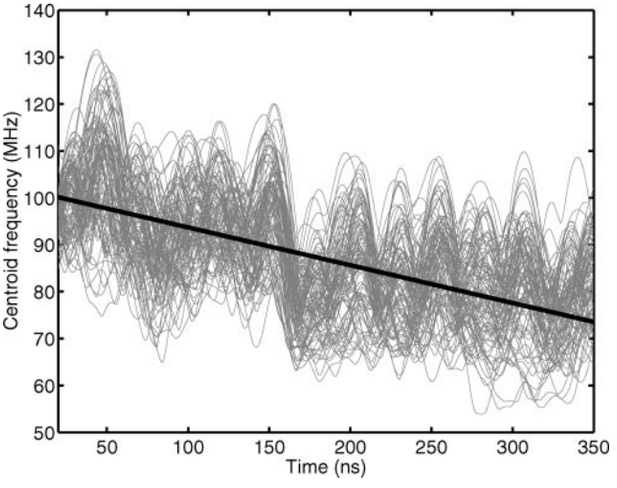

FIG. 8. Centroid frequency versus time curves for Langley data for traces between 100 and 120 m, before correcting for wavelet dispersion. Slope of best-fit line is −0.081 MHz/ns.

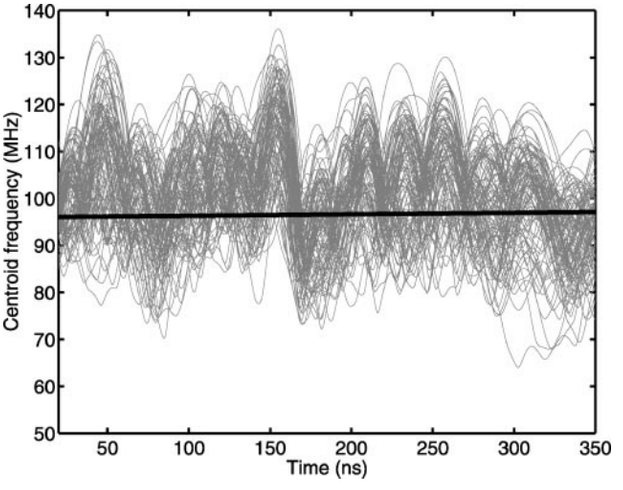

FIG. 10. Centroid frequency versus time curves for Langley data for traces between 100 and 120 m after correcting for wavelet dispersion. Best-fit line is approximately flat.

parameter C in equation (22), needed for the calculation of Q^*, we assume that the spectrum of the 100-MHz GPR source wavelet is approximately Gaussian in shape. Thus C can be determined from the spectrum variance, which should remain approximately constant during propagation (Quan and Harris, 1997). To estimate this parameter, variance values were computed from the S-transform results using a discretized version of equation (20). C was then computed from an average of those values near the beginning of the traces where signal-to-noise ratios were highest, the result being $C = 1170$. Using equation (22), the above results yield an estimate of $Q^* = 45$ for the sand and gravel aquifer.

Figure 9 shows the Langley data after inverse-Q filtering using $Q = 45$. There is a significant improvement in resolution compared with Figure 7; events in the GPR image are now "well-focused" in time and the widths of reflections at depth have been noticeably reduced. There are no visible signs of wavelet dispersion remaining in the inverse-Q filtered image. By examining the data in detail, it can also be seen that all events in Figure 9 correspond to events in Figure 7, and most can be followed laterally from trace to trace. This indicates that our inverse-Q filtering procedure has not produced any significant artifacts. The next logical processing step to further improve the resolution of the GPR image would be migration. The data in Figure 9 are in severe need of migration, as indicated by the numerous diffraction hyperbolas present in the profile.

After properly correcting for wavelet dispersion, the slope of a trace's centroid frequency versus time curve should theoretically be reduced to zero. Figure 10 shows the 100 centroid frequency versus time curves for the Langley data set from 100 to 120 m after inverse-Q filtering. A least-squares best-fit line through these curves is also shown. Indeed, the trend is nearly flat. It can thus be concluded that we have properly corrected for wavelet dispersion in the Langley data set. It should be noted that our value obtained for Q^* in this example is greater than the maximum value suggested by Turner and Siggins (1994). This suggests that the range for radar Q^* extends further than the range they propose.

CONCLUSIONS

In conclusion, the methods presented here, consisting of our adaptation of the frequency shift method and inverse-Q filtering, appear to provide a relatively robust and effective means of removing wavelet dispersion from GPR data. This allows us to significantly improve the resolution of the GPR image. Because our means of estimating Q^* avoids the need to isolate individual reflections on a trace, it possesses advantages over other more traditional methods for Q estimation. Further, our technique allows the reliable determination of whether or not we have properly removed wavelet dispersion from a data set; a properly corrected trace should show no general trend in the centroid frequency with time. Therefore, the absolute accuracy of our Q^* estimation method is not nearly as important as the fact that we can use it to get a first estimate of Q^*. This estimate can then be used as a starting point for inverse-Q filtering in an iterative procedure to properly correct for wavelet dispersion. As mentioned previously, signal processing techniques based on the assumption of a stationary wavelet, such as migration and spiking deconvolution, have been largely unsuccessful in the past when applied to GPR data. After correcting for wavelet dispersion, these techniques may allow us to successfully enhance even further the resolution of the GPR image.

It should be stressed that our adaptation of the frequency shift method is capable only of providing general estimates of Q^* in the subsurface; a high degree of resolution for Q^* with depth cannot be obtained. For this reason, the results of our Q^* estimation are best used for imaging purposes only and not for the identification of layer properties and interpretation. One means of overcoming these limitations might be to use borehole attenuation tomography methods as a means of obtaining more detailed estimates of subsurface Q^*. These could then be used as a basis for more accurate inverse Q filtering and also for identification/interpretation purposes.

ACKNOWLEDGMENTS

This research was supported in part by funding to R. Knight under Grant Number DE-FG07-96ER14711, Environmental Management Science Program, Office of Science and Technology, Office of Environmental Management, United States Department of Energy (DOE). However, any opinions, findings, conclusions, and recommendations expressed herein are solely those of the authors and do not necessarily reflect the views of DOE. J. Irving was supported through a Natural Sciences and Engineering Research Council of Canada (NSERC) postgraduate scholarship.

REFERENCES

Aki, K., and Richards, P. G., 1980, Quantitative seismology: Theory and methods: W. H. Freeman & Co.

Annan, A. P., 1996, Transmission dispersion and GPR: J. Envir. Eng. Geophys., **0**, 125–136.

Arcone, S. A., 1981, Distortion of model subsurface radar pulses in complex dielectrics: Radio Science, **16**, 855–864.

Baño, M., 1996a, Constant dielectric losses of ground-penetrating radar waves: Geophys. J. Internat., **124**, 279–288.

——— 1996b, Modeling and inverse Q imaging of ground penetrating radar waves in 1 and 2D: Geophys. Res. Lett., **23**, 3123–3126.

Berkhout, A. J., 1982, Seismic migration: Imaging of acoustic energy by wave field extrapolation, theoretical aspects: Elsevier Sci. Pub. Co.

Bickel, S. H., and Natarajan, R. R., 1985, Plane-wave Q deconvolution: Geophysics, **50**, 1426–1439.

Carcione, J. M., 1996, Ground-penetrating radar: Wave theory and numerical simulation in lossy anisotropic media: Geophysics, **61**, 1664–1677.

Cole, K. S., and Cole, R. H., 1941, Dispersion and absorption in dielectrics: J. Chemical Physics, **9**, 341–351.

Debye, P., 1945, Polar Molecules: Dover Publishing.

Deregowski, S. M., 1971, Optimum digital filtering and inverse filtering in the frequency domain: Geophys. Prosp., **19**, 729–768.

Fuller, B. D., and Ward, S. H., 1970, Linear system description of the electrical parameters of rocks: IEEE Trans. Geosci. Electronics, **GE-8**, 7–18.

Futterman, W. I., 1962, Dispersive body waves: J. Geophys. Res., **67**, 5279–5291.

Gabor, D., 1946, Theory of communications: J. IEE, **93**, 429–457.

Gladwin, M. T., and Stacey, F. D., 1974, Anelastic degradation of acoustic pulses in rock: Phys. Earth Plan. Int., **8**, 332–336.

Hollender, F., and Tillard, S., 1998, Modeling ground-penetrating radar wave propagation and reflection with the Jonscher parameterization: Geophysics, **63**, 1933–1942.

Jonscher, A. K., 1977, The 'universal' dielectric response: Nature, **267**, 673–679.

Keller, G. V., 1987, Rock and mineral properties, *in* Nabighian, M. N., Ed., Electromagnetic methods in applied geophysics: Soc. Expl. Geophys.

Kjartansson, E., 1979, Constant Q-wave propagation and attenuation: J. Geophys. Res., **84**, 4737–4748.

LaFlèche, P. T., Todoeschuck, J. P., Jensen, O. G., and Judge, A. S., 1991, Analysis of ground-probing radar data: Predictive deconvolution: Canadian Geotechnical J., **28**, 134–139.

O'Doherty, R. F., and Anstey, N. A., 1971, Reflections on amplitudes: Geophys. Prosp., **19**, 430–458.
Olhoeft, G. R., 1998, Electrical, magnetic, and geometric properties that determine ground penetrating radar performance: Proc. 7th Internat. Conf. on Ground Penetrating Radar, 177–182.
Olhoeft, G. R., and Capron, D. E., 1993, Laboratory measurements of the radio frequency electrical and magnetic properties of soils from Yuma, Arizona: U.S.G.S. Open-File Report **93-701**.
——— 1994, Petrophysical causes of electromagnetic dispersion: Proc. 5th Internat. Conf. Ground Penetrating Radar, 145–152.
Powers, M. H., 1995, Dispersive ground penetrating radar modeling in 2-D: Ph.D. diss., Colorado School of Mines.
Powers, M. H., and Olhoeft, G. R., 1994, Modeling dispersive ground penetrating radar data: Proc. 5th Internat. Conf. Ground Penetrating Radar, 173–183.
Quan, Y., and Harris, J. M., 1997, Seismic attenuation tomography using the frequency shift method: Geophysics, **62**, 895–905.
Rees, H. V., and Glover, J. M., 1992, Digital enhancement of ground probing radar data, *in* Pilon, J., Ed., Ground penetrating radar: Geo. Surv. Can. Paper **90-4**, 187–192.
Stacey, F. D., Gladwin, M. T., McKavanagh, B., Linde, A. T., and Hastie, L. M., 1975, Anelastic damping of acoustic and seismic pulses: Geophys. Surv., **2**, 133–151.
Stockwell, R. G., Mansinha, L., and Lowe, R. P., 1996, Localization of the complex spectrum: The S-transform: IEEE Trans. Signal Processing, **44**, 998–1001.
Strick, E., 1967, The determination of *Q*, dynamic viscosity, and creep curves from wave-propagation measurements: J. Geophys. Res., **13**, 197–218.
Taherian, M. R., Kenyon, W. E., and Safinya, K. A., 1990, Measurement of dielectric response of water-saturated rocks: Geophysics, **55**, 1530–1541.
Theophanis, S., and Queen, J., 2000, Color display of the localized spectrum: Geophysics, **65**, 1330–1340.
Toksöz, M. N., Johnston, D. H., and Timur, A., 1979, Attenuation of seismic waves in dry and saturated rocks: Laboratory measurements: Geophysics, **44**, 681–690.
Topp, G. C., Davis, J. L., and Annan, A. P., 1980, Electromagnetic determination of soil water content: Measurements in coaxial transmission lines: Water Resources Res., **16**, 574–582.
Turner, G., 1994, Subsurface radar propagation deconvolution: Geophysics, **59**, 215–223.
Turner, G., and Siggins, A. F., 1994, Constant *Q* attenuation of subsurface radar pulses: Geophysics, **59**, 1192–1200.
Varela, C. L., Rosa, A. L. R., and Ulrych, T. J., 1993, Modeling of attenuation and dispersion: Geophysics, **58**, 1167–1173.
von Hippel, A. R., 1962, Dielectrics and waves: John Wiley & Sons, Inc.
Xu, T., and McMechan, G. A., 1997, GPR attenuation and its numerical simulation in 2.5 dimensions: Geophysics, **62**, 403–414.